JOURNAL OF GEOPHYSICAL RESEARCH, VOL. 103, NO. A8, PAGES 17,543–17,557, AUGUST 1, 1998

Characteristics of the solar wind controlled auroral emissions

K. Liou, P. T. Newell, and C.-I. Meng

Applied Physics Laboratory, Johns Hopkins University, Laurel, Maryland

M. Brittnacher and G. Parks

Geophysics Program, University of Washington, Seattle

Abstract. We performed a high-time resolution (5 min) correlative study of the energy deposition rate in the northern auroral zone with the concurrent solar wind plasma and interplanetary magnetic field (IMF) observations for a 4 month period from March 30 to July 29, 1996. Auroral power, inferred by auroral emissions, was derived from images acquired by the ultraviolet imager (UVI) on board the Polar satellite, and the interplanetary parameters were based on Wind observations. It is found that dayside aurorae in the afternoon sector (65°-80° magnetic latitude (MLAT) and 1300-1800 magnetic local time (MLT)) are more active for large IMF cone angles and large solar wind electric fields. This result can be attributed to the manifestation of the antiparallel magnetic field merging in different locations and the partial "penetration" of the IMF on the dayside magnetopause. The integrated nightside (60°-75° MLAT and 2000-0100 MLT) auroral brightness is moderately correlated with the north-south component of the IMF and the solar wind speed with correlation coefficients of 0.49 and 0.35, respectively. The mean nightside auroral power is found to be approximately linearly proportional to the IMF B_z with a constant slope of 2 GW/nT. The solar wind speed, however, affects the nightside auroral power for both polarities of IMF B_z. Interestingly, the solar wind dynamic pressure shows no effect on the nightside auroral brightness. All these findings indicate that both reconnection and viscous-like interaction mechanisms play an important role in producing auroral emissions in the night sector. It is also found that the nightside auroral brightness responds to the southward turning of the IMF with a peak delay time of ~60 min. This result favors the model of loading-unloading magnetosphere. We also found that a negative IMF B_y condition favors the nightside auroral activity, and we attributed this effect to the partial penetration of the IMF B_y. Finally, the response function for nightside aurora is given as $\sim VB_T^4 \sin^4(\theta_c/2)$ with a median correlation coefficient of 0.63, indicating that there may be other factors other than the solar wind and IMF responsible for lightening up the northern-southern hemispheric sky.

1. Introduction

The study of global morphology of aurora is often driven by the belief that auroral features seen at the low-altitude ionosphere can be used to infer auroral processes taking place in high-altitude magnetospheric regions. For example, the distribution of optical aurora has been known to be closely related to the Birkeland field-aligned currents for quite some time. Through the use of an extensive database acquired from the Greenland all-sky camera network, *Danielsen* [1980] found that the region of possible occurrence of discrete aurora is coincident with the statistical region 1 field-aligned currents generated in the magnetosphere [*Iijima and Potemra*, 1976]. It has also been reported that as geomagnetic activity increases, the Birkeland field-aligned currents increase [*Sugiura and Potemra*, 1976] as well as the occurrence rate of discrete aurorae [*Danielsen*, 1980], indicating that the aurora is an integral part of geomagnetic activity resulting from the solar wind-magnetosphere-ionosphere coupling.

As the magnetosphere responds to changes in the solar wind, in particular the interplanetary magnetic field (IMF), the configuration of the magnetosphere changes. This may therefore change the configuration of aurora seen in the ionosphere. It is believed that changes in the

Paper number 98JA01388.
0148-0227/98/98JA-01388$09.00

solar wind flow near the magnetopause, and the convection flow inside the magnetosphere will change the intensities of field-aligned currents and therefore change the intensities of aurora. Evidence of this is given by *Lassen and Danielsen* [1978] who used an extensive database acquired by the Greenland all-sky camera network to study the statistical distribution of auroral arcs under different IMF orientations and found that oval arcs occurrence rate and the size of the auroral oval is closely related to the z component of IMF. In general, they found that the arc occurrence rate is higher when the IMF B_z is southward; as B_z turns northward, occurrence rate of arcs decreases, and the auroral oval contracts. The size of auroral oval was also found to be correlated with the magnitude of the negative IMF B_z [*Holzworth and Meng*, 1975]. Satellite global auroral observations have also shown temporal and spatial responses of aurora to the solar wind variations. *Murphree and Elphinstone* [1988], through analyzing the global auroral images acquired by the ultraviolet imager on board the Viking satellite, reported that during positive IMF B_z and away sector configurations, localized regions of auroral emission on the dayside can propagate either duskward or dawnward depending on the sign of IMF B_y. This is usually linked to the response of convection pattern to the y component of IMF when reconnection is at work. A further study of the Viking UV imagery by *Elphinstone et al.* [1990] also indicated that high-latitude auroral arcs in the dusk sector occur for positive IMF B_y, while negative B_y gives dawn sector polar arcs during a B_z northward condition.

The IMF B_y is thought to affect the dayside auroral morphology most. Early case studies have shown that transient auroral events moving eastward or westward in the midday sector are controlled by the polarity of IMF B_y [*Sandholt et al.*, 1986]. A recent statistical study performed by *Karlson et al.* [1996] indicated that an asymmetric prenoon-postnoon auroral occurrence distribution is caused by the IMF B_y polarity during negative IMF B_z. It is found that postnoon (1200-1400 magnetic local time (MLT)) auroral events are more frequent than prenoon (1000-1200 MLT) auroral events for negative IMF B_y, while the trend is reversed for positive IMF B_y. This local time distribution of dayside aurorae caused by the sign of IMF B_y is opposite to the displacement of the cusp found in particle precipitation [*Newell et al.*, 1989].

Early auroral researchers have mainly relied on the ground all-sky camera observations to study auroral morphology. This type of observation is subject to a very limited field of view and therefore is not suitable for quantitative auroral research in global or even mesoscale phenomena. Even with the satellite global auroral imagers which have been available for ~20 years, reports of quantitative analysis of large-scale aurorae are still rare. This sometimes makes a direct comparison between different measurement results impossible. In the present paper we take the advantage of the large database returned by Polar ultraviolet imager (UVI) to study the characteristics of dayside and nightside aurorae under various solar wind plasma and IMF conditions. Contrary to many previous qualitative works, we will concentrate on how the solar wind influences the auroral emission in a quantitative approach. Since the brightness of auroral radiation is a measure of the rate of energy deposition into the atmosphere due to electron precipitation, results of this study can be used to infer the total energy of electron precipitating into the auroral zone. Another prime interest of this study is to quantify the auroral power as a function of interplanetary parameters to provide a useful knowledge for space weather forecasting.

A number of works have indicated that an auroral oval consists of two different arc systems, dayside and nightside, powered by different dynamo mechanisms [*Akasofu and Kan*, 1980; *Meng and Lundin*, 1986; *Lui et al.*, 1989; *Brittnacher et al.*, 1997]. The nightside aurora is usually associated with large-geomagnetic activities such as magnetic storms and substorms and therefore is believed to be controlled by the southward turning of the IMF and magnetic field line reconnection in the tail region. The postnoon aurora is transient in nature and is found to be collocated with the region 1 upward field-aligned currents associated with precipitating electrons with energies below 1 keV [*Newell et al.*, 1996b]. The source of dayside aurora in the afternoon region is still an open question. The persistent and sometimes spatially periodic features of the postnoon aurora favor models associated with the Kelvin-Helmholtz instability which is created by the shearing of the solar wind flow on the flanks of magnetopause [*Lui et al.*, 1989; *Vo and Murphree*, 1995]. A recent statistical study of the intensification of the postnoon auroral bright spots with the Polar ultraviolet imagery by *Liou et al.* [1997a] further substantiates that postnoon aurorae are distinct features from the nightside auroral substorms. For this reason, we will address the response of dayside and nightside aurorae to the solar wind plasma and IMF parameters separately.

The remainder of this paper is organized as follows: Section 2 explains how the Polar UVI and Wind plasma and IMF data were processed for analysis. Section 3 presents data analysis with emphasis on the afternoon and the premidnight sectors. Discussion and summary and conclusion will be given in section 4 and section 5, respectively.

2. Data Preparation

This study utilizes Polar UVI image data and Wind solar wind plasma and IMF measurements for a time period between March 30 and July 29, 1996. The Polar UVI has returned a large number of images of the north auroral region. The total number of useful images sampled at the long Lyman-Birge-Hopfield (LBH-long) band (~1700 Å ± 50 Å) and at the 36 s exposure time is

estimated at ~18,130 with at least 80% of the northern auroral regions coverage and a time separation of ~5 min between two consecutive images under the normal observational mode (see *Torr et al.* [1995], for detail information about the UVI). The interplanetary parameters used for this study are the solar wind velocity and density acquired by the solar wind experiment [*Ogilvie et al.*, 1995] and the interplanetary magnetic fields acquired by the magnetic fields investigation [*Lepping et al.*, 1995] on board the Wind spacecraft. The 1 min in IMF and 2 min in solar wind plasma key parameter data are provided by the Data Distribution Facility at NASA Goddard Space Flight Center. The Wind spacecraft spends most of its time in the solar wind ~200 R_E upstream of the Earth's bow shock, and therefore it can provide a continuous monitoring of the solar wind plasma and IMF. There is a disadvantage in using the Wind data for correlative studies, however, because the Wind spacecraft is located too far from the Earth, and complex structure and transient nature of the solar wind often make the prediction of the solar wind event observed by Wind propagating to the Earth unreliable. Therefore a reduction in the correlation should be expected.

A series of several steps was required to prepare a data set suitable for analysis. The UVI's instrument counts are first converted to photon flux at the imager aperture with calibration data [*Brittnacher et al.*, 1997]. After correcting for the Van Rhijn effect due to unequal optical lengths in the field of view and subtracting the dayglow, one can derive the auroral surface brightness in Rayleighs. A detail description of the procedure is given by *Liou et al.* [1997b]. Filtered images at the LBH-long band will be used for this study because at this wavelength, auroral emission is approximately proportional to the electron precipitating energy density flux [*Strickland et al.*, 1993; *Germany et al.*, 1994]. The conversion of surface brightness in Rayleighs to ergs cm^{-2} s^{-1} for the UVI LBH-long band has been modeled by *Germany et al.* [1997] and is given as 1 erg cm^{-2} s^{-1} $\approx$ 110 Rayleighs. In this study, postnoon and nightside aurorae will be considered separately. The postnoon aurora is defined by a region approximately along the auroral oval between 1300 and 1800 MLT and 65° and 80° magnetic latitude (MLAT) while the nightside region is between 2000 and 0100 MLT and 60° and 75° MLAT [cf. *Newell et al.*, 1996a, b; *Liou et al.*, 1997b]. The total energy-deposited rate (power in gigawatts) is then derived by integrating the energy density flux over the area defined for the dayside and nightside regions.

The interplanetary parameters were first averaged by a 5 min moving window and then time shifted to account for the transit time of the solar wind from the observation site of the Wind spacecraft to the Earth's bow shock subsolar point. Since solar wind features tend to be aligned with the IMF, the transit time can be approximated by $\tau_{\text{transit}} = (X_{\text{SC}} - X_{\text{BS}} - \rho \times B_x/B_\rho)/V_{\text{SW}}$, where X_{SC} is the corrdinate of the Wind spacecraft along the Earth-Sun line in GSM, X_{BS} is the coordinate of the subsolar bow shock and is taken to be 14.6 R_E [*Fairfield*, 1971], $\rho = \sqrt{Y^2 + Z^2}$ is the perpendicular distance from the Earth-Sun line to the spacecraft in the X-Y plane, $B_\rho = (B_y \times Y + B_z \times Z)/\rho$, and V_{SW} is the speed of solar wind. This approximation is limited to median IMF cone angles between 45° and 135° only. For small ($\leq$ 45°) and large ($\geq$ 135°) IMF cone angles, we simply use 45° and 135° to approximate the IMF orientation, respectively. The total propagation time that should pass before an effect is seen in the ionosphere is then estimated to be the sum of the transit time τ_{transit} calculated above + 5 min for traversing the magnetosheath and 2 min Alfven transit time [*Lockwood et al.*, 1989] to reach the ionosphere.

3. Data Analysis and Results

In order to study the dependence of auroral power on the interplanetary parameters, the large-auroral database is binned by solar wind plasma and IMF parameters to show the average trend of the auroral brightness under various conditions. With a relatively limited short time coverage (4 months) of our database, interplanetary parameters may show intercorrelation which can affect the interpretation of the results. Therefore it is useful to discuss the intercorrelation between variables before proceeding to the data analysis. The correlation matrix of the six interplanetary parameters is shown in Table 1 for $B_z < 0$ (upper triangle) and $B_z > 0$ (lower triangle). It has been well known that solar wind dynamic pressure variation mainly results from variations in the solar wind density, and this high correlation is also shown in our surveyed database, r = 0.9/0.83 for $B_z > 0/B_z < 0$. A median correlation coefficient, r = -0.43/-0.3, between B_x and B_y is consistent with what we found separately that in slightly <50% of this surveyed period the IMF is in the garden hose orientation. The solar wind density shows a median correlation with the positive IMF B_z (r = 0.40) and a median anticorrelation with the solar wind speed (r = - 0.42/- 0.49). The surveyed Wind data set also shows a small to median correlation between the solar wind speed and B_x for $B_z > 0$ (r = 0.35) and between the solar wind dynamic pressure and the IMF B_z (r = 0.39/-0.21).

Table 1. Correlation Matrix for $B_z > 0$ and $B_z < 0$

	B_x	B_y	B_z	V	N	P
B_x		-0.30	0.12	0.10	-0.19	-0.17
B_y	-0.43		-0.00	-0.01	0.05	0.05
B_z	-0.07	0.19		-0.08	-0.12	-0.21
V	0.35	-0.16	-0.11		-0.49	-0.02
N	-0.08	0.19	0.40	-0.42		0.83
P	0.04	0.12	0.39	-0.04	0.90	

$B_z > 0$, lower triangle; $B_z < 0$, upper triangle.

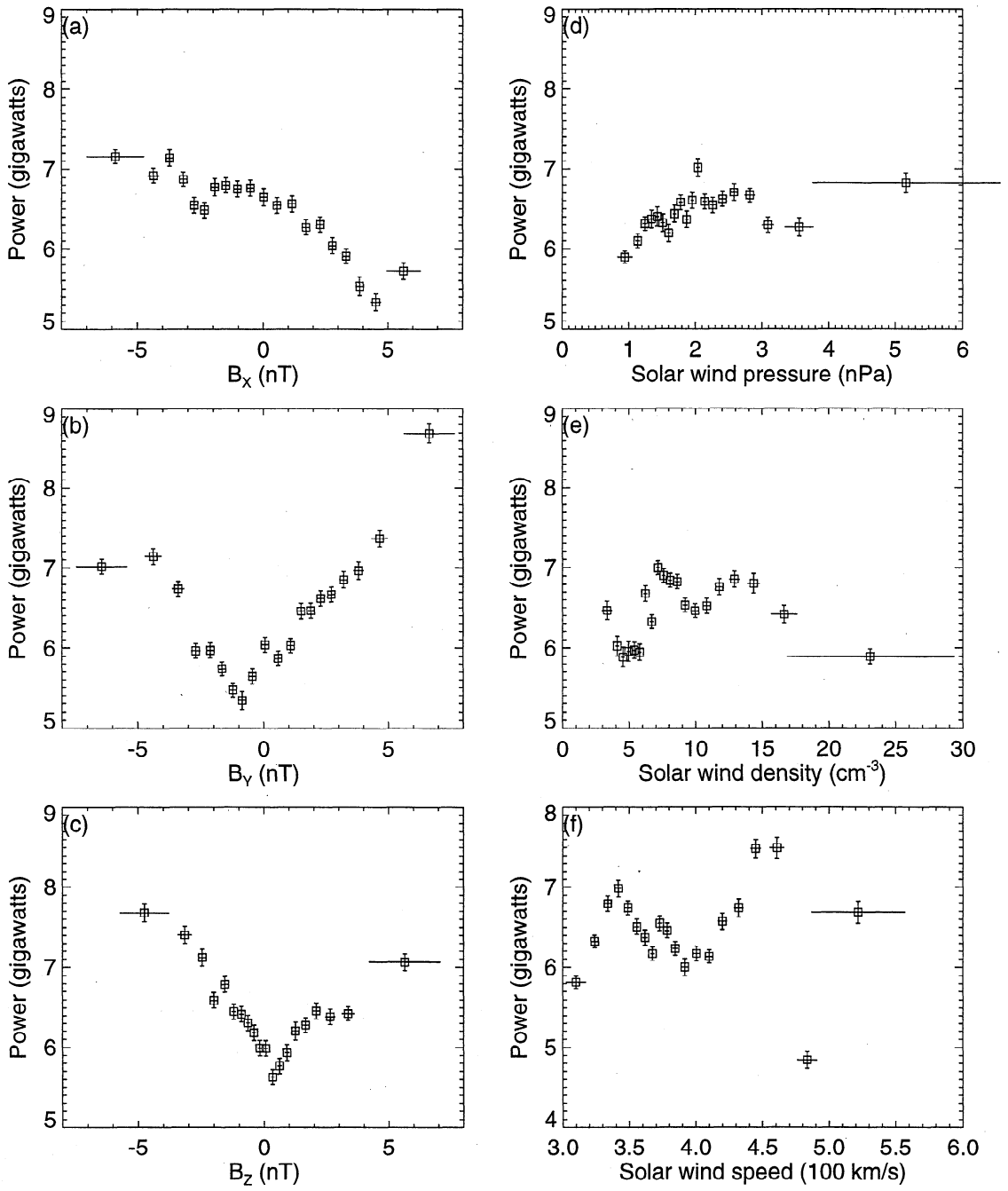

Figure 1. Response of afternoon (65°-80° MLAT and 1300-1800 MLT) auroral energy deposition rate in gigawatts to (a) IMF B_x, (b) IMF B_y, (c) IMF B_z, (d) solar wind dynamic pressure, (e) solar wind density, and (f) solar wind speed.

3.1. Dayside Aurora

3.1.1. Effect of Solar Wind Plasma and IMF parameters. To illustrate the solar wind plasma and IMF effects on the total afternoon auroral power along the oval, a total of 10,843 valid images are binned by the three components of IMF, solar wind dynamic pressure, density, and speed, and the result is shown in Figures 1a-1f as square boxes. The vertical error bars representing 1 s.d. from the mean are provided. Since the size of bins is irregular (measurements are equally distributed in each bin), horizontal error bars are also provided in the figure. The x component of the IMF shows trend toward increasing auroral power as the IMF B_x changes from a toward (with respect to the Sun) to an away configuration. This increase in northern hemispheric auroral power is estimated to be ~40% from 5 GW (B_x = 5 nT) to 7 GW (B_x = -5 nT). The afternoon auroral power shows a positive response to an increasing IMF B_y magnitude. This increase is approximately symmetric about B_y = -1 nT but with a much brighter afternoon aurora for large $+B_y$. Similarly, postnoon aurorae

appear to be affected by the z component of the IMF in the same way the IMF B_y does; that is, auroral brightness increases with $|B_z|$ but less dramatic for $B_z > 0$ than for $B_z < 0$.

The response of afternoon auroral power to the solar wind parameters, Figures 1d-1f, is not as evident as that to the IMF. Although a small increase in auroral power occurs for an increase of solar wind dynamic pressure, this increase is small and occurs in a very low pressure region. The solar wind density which is highly correlated with the solar wind dynamic pressure (see Table 1) does not show any effect on the dayside aurora either. It is worthwhile to note that we also found a few high-power events (>10 GW) which occurred at very high dynamic pressure (P > 10 nPa) and high density (N > 40 cm^{-3}) during storm times, but we don't think this is statistically significant. The most interesting and unexpected result is the lack of dependence of the afternoon aurora to the solar wind speed. This can be seen from Figure 1f which shows a random and highly scattered distribution of the afternoon auroral power over the entire solar wind speed range. Since the correlation between the solar wind density and speed is found to be low (r $\approx$ -0.45), the lack of dependence of dayside aurora on the solar wind parameters cannot be due to special distribution (intercorrelation) between the solar wind density and speed which often occurs in statistical studies with a small database.

3.1.2. IMF Cone-Angle Effect. We have shown that the postnoon auroral power is controlled by the IMF mainly through the transverse component of IMF, $B_T = \sqrt{B_y^2 + B_z^2}$ and the IMF B_x. A combination of these two parameters is the IMF cone angle defined by $\theta = \tan^{-1}(B_T/B_x)$, which should also show effects on the dayside aurora. In Figure 2, postnoon auroral power is binned by the IMF cone angles for all IMF B_z (solid line), $B_z > 0$ (dashed line), and $B_z < 0$ (dotted line). Again, 1 s.d. from the mean is plotted as vertical error bars. The horizontal error bars correspond to 1 s.d. and roughly represent the size of the bins. Figure 2 shows that dayside auroral power increases with the IMF cone angle and peaks around 100° (not 90°), followed by a slight decrease at larger angles. Although negative IMF B_z always results in more aurora, the difference between $B_z > 0$ and $B_z < 0$ is ~8% on average. It is worth noting that the minimum power doesn't approach zero at zero IMF cone angle. If we extrapolate the dashed line down to zero cone angle, the total power is ~3 GW, the apparent basal auroral power in the afternoon.

3.1.3. Dependence on solar wind electric field and energy. In light of a strong dependence of the dayside aurora on the IMF and a weak dependence on the solar wind parameters, one naturally would suspect that the solar wind electric field and/or the solar wind magnetic field energy are the two most important physical quantities that involve the solar wind-magnetosphere interaction contributing the dayside aurora. A simple test of this idea is given in Figure 3, in which the precipitation power is binned by solar wind electric field, $V \times B$, solar wind kinetic energy flux, $\rho V^3/2$, and IMF magnetic energy flux, $VB^2/8\pi$. The dependence of the afternoon aurora on the transverse component of the IMF, B_T, is also shown in Figure 3a for a comparison. For all three physical quantities, the electric field and the solar wind magnetic energy density flux do fit better than the solar wind kinetic energy density flux as expected, with the electric field revealing a slightly better correlation with the mean dayside aurora ($r = 0.98$). Note that a high correlation with the mean auroral output does not imply a high correlation with the sample population. Indeed the latter correlation is far lower ($r = 0.32$).

3.2. Nightside Aurora

3.2.1. Multiple Regression. To illustrate what are the interplanetary parameters which may influence the nightside auroral activities, we first use the multiple linear regression technique to examine the basic parameters: three components of the IMF, solar wind speed, density, and solar wind dynamic pressure. This allows us to obtain the relative weight in contributing

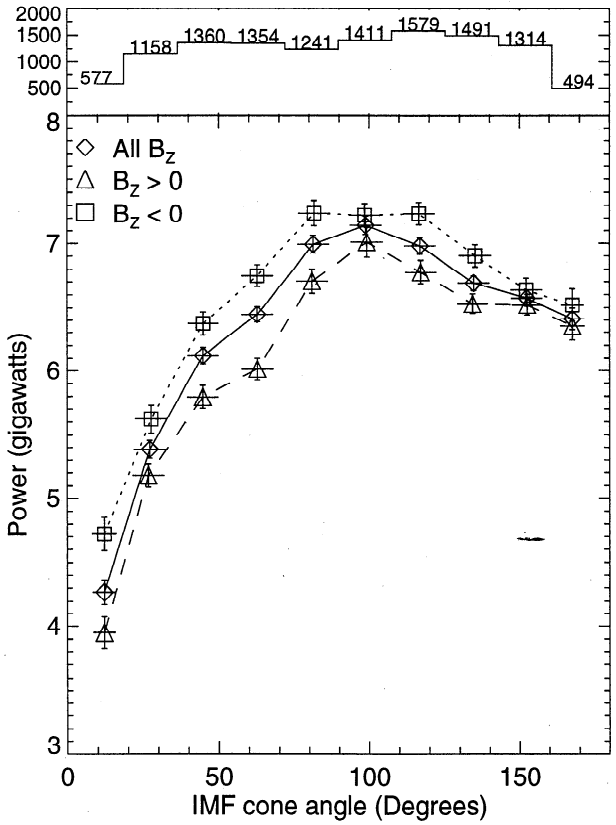

Figure 2. Response of afternoon auroral power in gigawatts in the postnoon section (65°-80° MLT and 1300-1800 MLT) to IMF cone angle for $B_z > 0$ (dashed line), $B_z < 0$ (dotted line), and all B_z (solid line). The number of images binned by each bin is given on the top of figure.

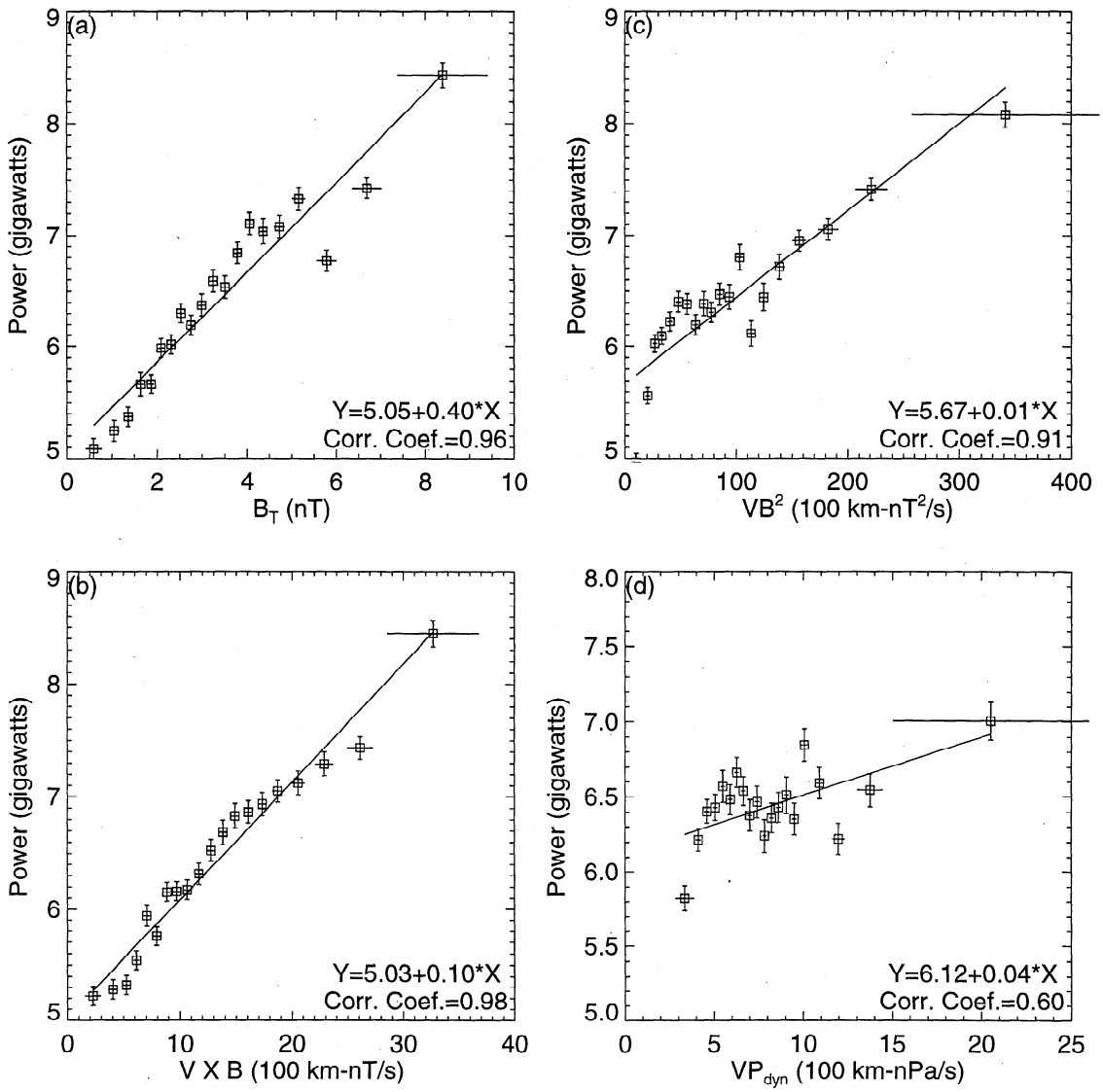

Figure 3. Response of auroral power in gigawatts in the postnoon sector (65°-80° MLAT and 1300-1800 MLT) to the transverse component of (a) IMF, B_T, (b) solar wind electric field, $V \times B$, (c) solar wind magnetic energy density flux, VB^2, and (d) kinetic energy density flux, $VP_{\rm dyn}$.

the nightside auroral activities and later to help construct more complex forms of possible response function. The multiple regression was performed for northward IMF and southward IMF conditions and the result is shown in Table 2. The first row in Table 2 lists the coefficients of the linear regression form. In general, a larger regression coefficient represents a better correlation. The second and third rows in Table 2 list the correlation coefficients and standard deviations, respectively. By examining the correlation coefficient we can determine which parameters affect aurora most. In our test, all correlation coefficients were significant to >99.999% confidence level or, equivalently, there was <0.001% chance that the correlation was random. We also divided the entire data set randomly into two parts and performed linear regression analysis on each subset.

Table 2. Multiple Linear Regression for $B_z > 0/B_z < 0$

	B_x	B_y	B_z	V	N	P
Coef.	-.095/-.122	-.075/-.251	-.160/-1.05	3.732/6.40	-.123/-.021	.806/.800
R	.045/-.059	-.092/-.136	-.095/-.361	.305/.341	-.088/.003	.050/.219
Sigma	.013/.018	.014/.018	.024/-.041	.456/.553	.031/.049	.138/.212

N = 18,130, R = 0.508, and $\chi^2 = 10.65$. Coef. is coefficient.

We found the correlation coefficient for both subsets was close to that of the entire data set within 10% uncertainty (not shown). When the IMF is northward, all correlation coefficients are less 0.1 except the solar wind speed which shows a relatively high correlation of 0.3. This may indicate that when reconnection is inactive, aurorae are caused by fluid interaction instabilities of the solar wind flowing around the magnetosphere cavity as predicted in the closed model [*Axford and Hines*, 1961]. When reconnection is active; that is, $B_z < 0$, a dramatic change in correlation coefficients can be seen in Table 2. The y and z components of the IMF and the solar wind dynamic pressure became more or less correlated with the nightside auroral power. The IMF B_z parameter reveals the greatest response to the nightside aurora followed by the solar wind dynamic pressure and IMF B_y. This can be explained as more energy coupling due to magnetic field reconnection predicted by the open model [*Dungey*, 1961]. The slight increase in B_y correlation coefficient suggests that the IMF clock angle may play an important role in reconnection. The solar wind speed has long been considered as one of the important parameters involving the solar wind-magnetosphere energy coupling process. The correlation coefficient for the solar wind speed decreases but not significantly, indicating that the solar wind speed contributes the solar wind-magnetosphere energy coupling in all states of the magnetosphere.

3.2.2. Response Time. It has been reported that the auroral electrojet index, AE, reveals a maximum response to the IMF B_z when the IMF B_z was lagged for a time from ~40 min [*Meng et al.*, 1973] to 60 min [*Arnoldy*, 1971]. A 30-50 min delay between isolated substorms, indicated by the AE index, and VB_z has also been reported by *Rostoker et al.* [1972]. This long time delay between the southward turning of IMF and the AE index is usually interpreted as a loading model of the magnetosphere. Auroral substorms, which contribute the major energy deposition from the magnetosphere into the nightside auroral oval, are believed to be closely correlated with the magnetic substorms and therefore must reveal a delay. Here we will investigate this time delay issue using the nightside aurora. Again, the time axis of the solar wind parameters was shifted forward (add time) from 0 to 100 min with a 10 min increment. For each shift, we calculate correlation coefficients for all six solar wind parameters, and the result is shown in Figure 4. We have also divided the entire data set into two subsets randomly and recalculated the correlation coefficients for different lag times; the result is also shown as dotted and dashed lines in Figure 4. Although all the correlation coefficients appear to be low, the difference between the subsets and the entire data set is well <10%, indicating this result is statistically significant. Basically, the correlation coefficient of all parameters do not change with the lag time except for the z component of the IMF, which reveals a maximum anticorrelation (negative correlation coefficients) around 60 min. When the data set is divided into two parts according to the polarity of the north-south component of IMF, the time lag response for the solar wind speed changes. When the IMF B_z is northward, there is a minimum response around 40-50 min, while $B_z < 0$, the response in solar wind velocity maximizes at 50 min. Although the changes in correlation for both cases are not significant (~12%), it may suggest that under slow merging conditions (the magnetosphere is almost always at least partly open) the solar wind-magnetosphere is a direct driven system. In a rapid merging condition, $B_z < 0$, the solar wind-magnetosphere is a loading-unloading system.

3.2.3. Effect of the Solar Wind Plasma and IMF parameters. Figure 5 illustrates the response of the nightside auroral power delayed by 60 min to the solar wind and IMF parameters. Again, the vertical error bars corresponding to 1 s.d. from the mean and the horizontal error bars representing 1 s.d. are also provided because of the use of an uneven size of bins. In general, Figure 5 is consistent with the correlation result listed in Table 2. As expected from the low correlation coefficient, the IMF B_x does not show a systematic effect on

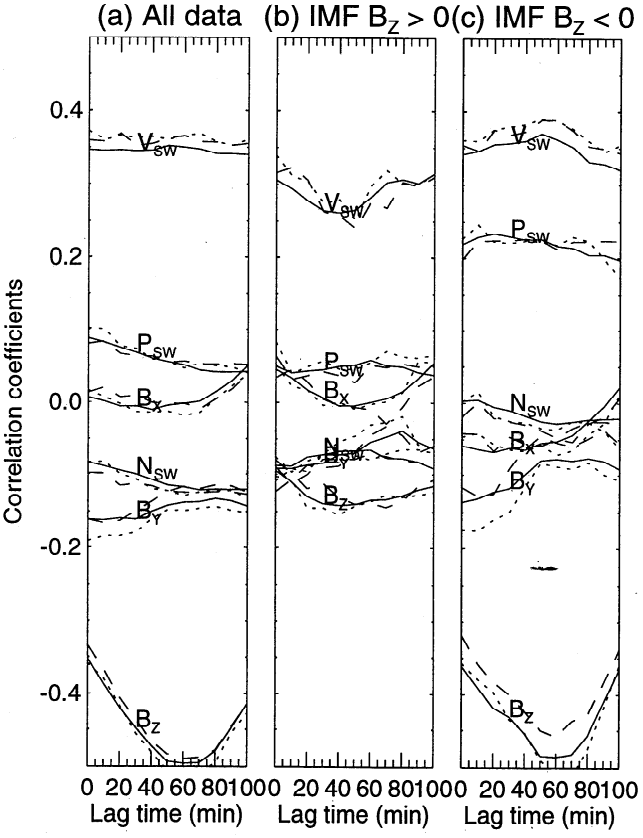

Figure 4. Lagged cross-correlation analysis for six solar wind plasma and IMF parameters and nightside (60°-75° MLAT and 2000-0100 MLT) auroral power variations for (a) entire data set, (b) $B_z > 0$, and (c) $B_z < 0$. In each figure, the solid lines represent the whole data set while the dotted lines and dashed lines represent two randomly divided data subsets.

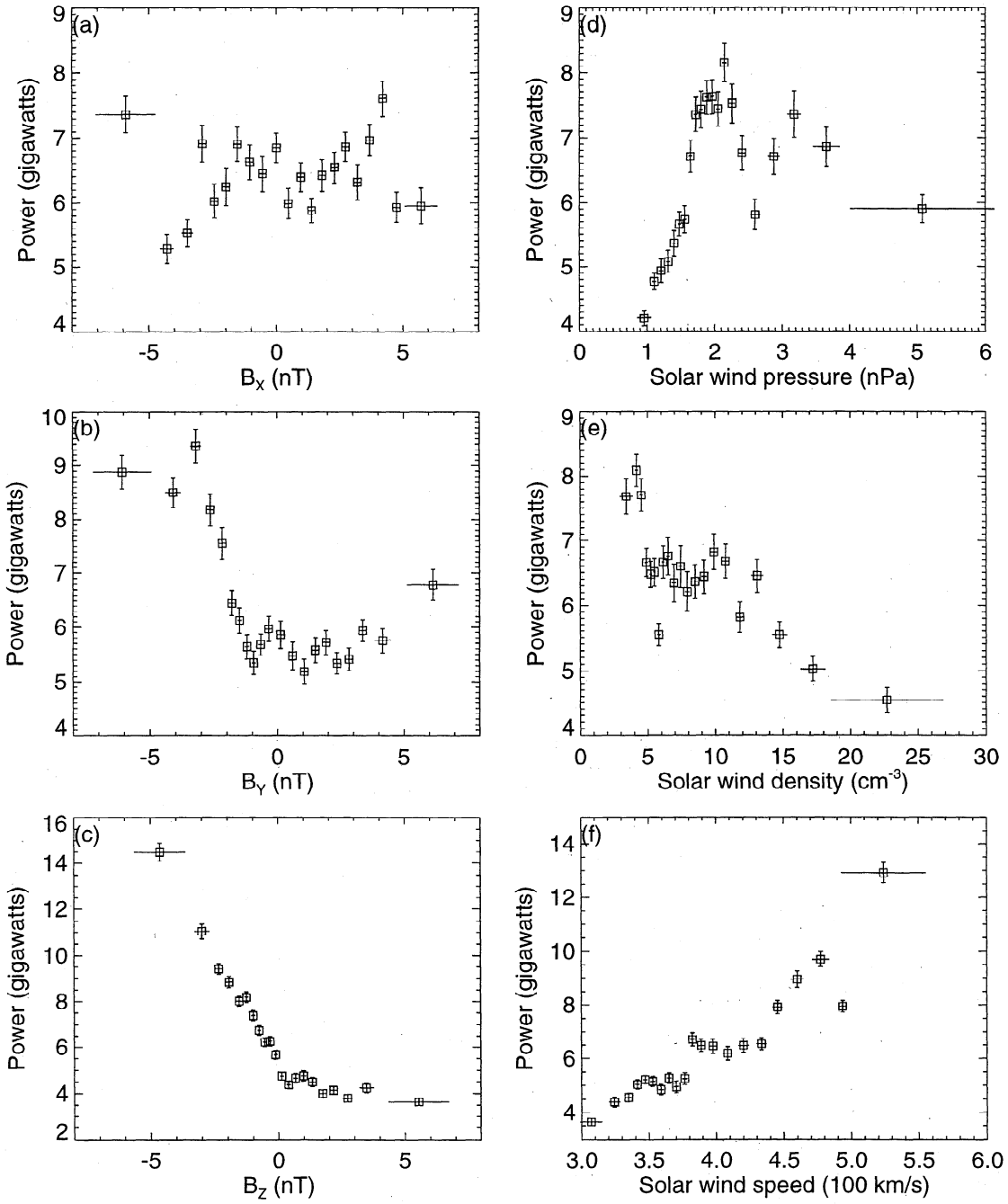

Figure 5. Response of auroral power in gigawatts in the midnight sector (60°-75° MLAT and 2000-0100 MLT) to six solar wind plasma and IMF parameters.

the nightside aurora. The IMF B_y has a minimal effect on the nightside aurora for small values of $|B_y|$. Although the auroral power increases with the IMF $|B_y|$, it appears to be much brighter for $B_y < 0$. The average total nightside auroral emission is well-predicted by the IMF B_z as one would expect. The auroral emission is low and relatively independent of the strength of B_z for $B_z > 0$, but it increases linearly with the magnitude of the B_z for $B_z < 0$. The basal emission is estimated at ~3.5 GW ($B_z > 5$ nT) and the slope for $B_z < 0$ is ~2 GW/nT. The transition from positive B_z to negative B_z is not step function-like; however, as one can see from Figure 5c that the auroral emission starts increasing slowly around $B_z = 2$ nT. This result may suggest that reconnection plays a dominant role in controlling energy coupling between the solar wind and the magnetosphere as predicted by the open model [*Dungey*, 1961]. However, the basal emission which is independent of the orientation of the B_z may be attributed to a model in which the solar wind energy is delivered by

the frictional solar wind flow, which enters the magnetosphere from the low-latitude magnetosphere boundary layer via viscous interactions.

Among the solar wind parameters the solar wind dynamic pressure and density do not show a consistent and systematic relation with the nightside aurora. Although a sharp monotonic increase in the auroral power occurs for the solar wind dynamic pressure below 2 nPa, this correlation fails at higher pressures. The nightside aurora shows a trend of decreasing in power with the solar wind density, but the majority of the measurements between 5-10 cm^{-3} stay unchanged (6-7 GW). Moreover, we expect a similar trend on the auroral power for the solar wind dynamic pressure and density because both parameters are highly correlated. A clear enhancement of the nightside auroral power due to the increase of the solar wind speed is shown in Figure 5e, as is expected owing to a high-correlation coefficient given in Figure 4. However, the relatively large spread of the mean values (as also shown in Table 2) may cast a doubt about this linear relationship. To further illustrate the solar wind speed effect, we have plotted the nightside auroral power, binned by regular bins of 1 nT in bin size, versus the IMF B_z for three different solar wind speed ranges separated by V = 360 km s^{-1} and V = 420 km s^{-1} in Figure 6. The dashed/dotted line representing the

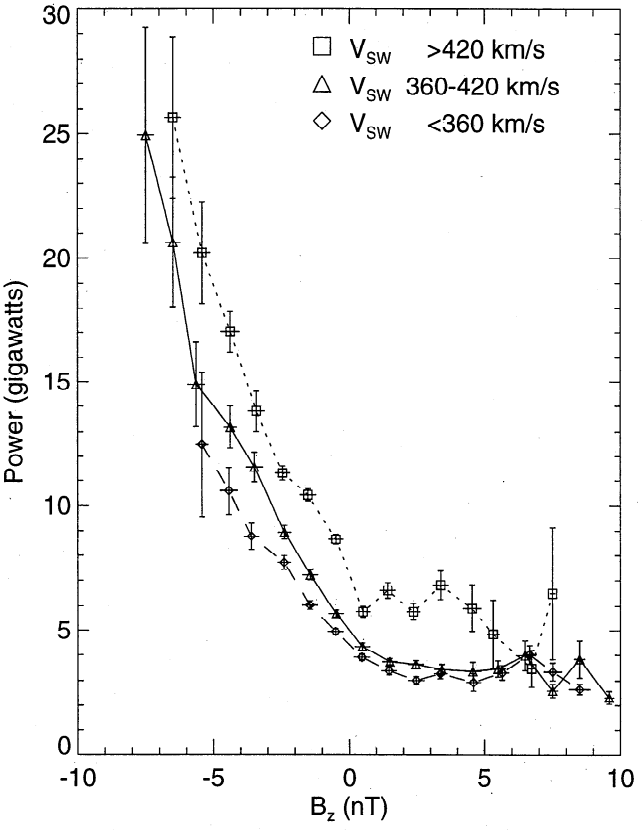

Figure 6. Response of auroral power in gigawatts in the midnight sector (60°-75° MLAT and 2000-0100 MLT) to the z component of IMF for three different solar wind speed ranges.

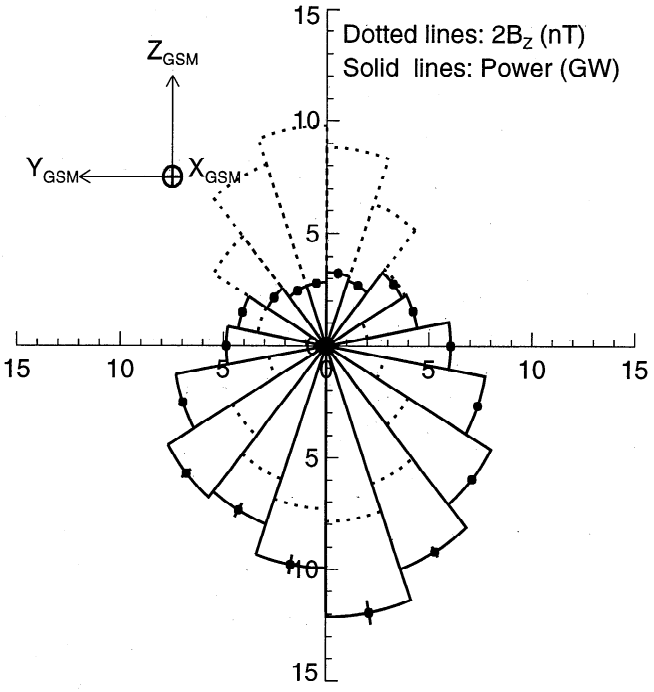

Figure 7. Response of auroral power in the midnight sector (60°-75° MLAT and 2000-0100 MLT) to IMF clock angle (solid lines). The dotted lines represent 2 times of IMF B_z as a function of IMF clock angle.

low/high solar wind speed reveals the smallest/highest power for all B_z range except for $B_z > 6$ nT, where uncertainty is large. Interestingly, this increase in power due to the increase of solar wind speed is approximately linear for $B_z < 0$ and non-linear for $B_z > 0$.

3.2.4. IMF clock angle effect. Although the nightside auroral power is strongly correlated with the negative component of the IMF B_z, a weak correlation with the IMF B_y shown in Table 2 indicates that the nightside auroral power may be IMF orientation dependent; that is , the relationship is not a simple half-wave rectifier model. To show this dependence, we have binned the nightside auroral power by the IMF clock angle with 20° bins of equal size and the result is shown as solid lines in Figure 7, where the error bars are 1 s.d. from the mean and the dotted lines show twice the magnitude of the IMF B_z. Normally, the IMF clock angle is measured from the $+z$ GSM axis clockwise or anticlockwise to the $-z$ GSM axis without considering the sign of the B_y. Since the nightside aurora favors negative B_y conditions and in order to show the auroral response to different signs of IMF B_y, we have separated the IMF clock angle for different signs of B_y. In Figure 7 one can see that auroral power shows minimal when the IMF clock angle is close to 0° and then increases with the increase of the IMF clock angle from either sign of B_y. When B_y is negative, auroral power is larger than that when B_y is positive but by only a factor of ~15-20% on average. Since auroral power is linearly proportional to the IMF $|B_z|$, to further illustrate the

Table 3. Correlation Coefficients of Nightside Auroral Power

Coupling functions	0 min	60 min	References
B_z	-0.35	-0.50	*Arnoldy* [1971]
VB_z	-0.37	-0.52	*Rostoker et al.* [1972], *Burton et al.* [1975]
VB_T	0.20	0.25	*Doyle and Burke* [1983]
V^2B_z	-0.38	-0.53	*Murayama and Hakamada* [1975]
VB_z^2	0.07	0.07	*Baker et al.* [1981]
$VB_T\sin(\theta_c/2)$	0.39	0.53	*Gonzalez and Mozer* [1974]
$VB_T\sin^2(\theta_c/2)$	0.44	0.60	*Kan and Lee* [1979]
$VB_T\sin^4(\theta_c/2)$	0.46	0.63	*Wygant et al.* [1983]
$VB^2\sin^4(\theta_c/2)$	0.43	0.55	*Perreault and Akasofu* [1978]
$P^{1/2}VB_z$	-0.34	-0.47	*Murayama* [1982], *Gonzalez* [1990]
$P^{1/3}VB_T^2\sin^4(\theta_c/2)$	0.38	0.54	*Vasyliunas et al.* [1982]
$P^{1/6}VB_T\sin^4(\theta_c/2)$	0.46	0.63	*Vasyliunas et al.* [1982]

B_y effect, we have also plotted the IMF $|B_z|$ in Figure 7 as dotted lines for a comparison. In general, the average IMF B_z is about the same for the same IMF clock angles of either sign of B_y. Actually, the total IMF B_z, summed by each bin, is slightly larger for $+B_y$ than for $-B_y$.

3.2.5. Response Function. Many empirical solar wind-magnetosphere energy coupling functions have been proposed as a proxy of energy input [see, e.g., *Vasyliunas et al.*, 1982, and references therein]. The most often used energy proxies are geomagnetic indices, such as the auroral electrojet current indices, *AE* (*AU* and *AL*), measured on the ground [*Maezawa*, 1979; *Murayama*, 1982; *Baker*, 1986] and the cross-polar cap potential measured at high altitude [*Reiff et al.*, 1981]. Auroral particle energy precipitation directly measured by DMSP satellite has also been used to fit a response function, a combination of the IMF B_z, and solar wind speed [*Brautigam et al.*, 1991]. In this section, we will find a response function for the auroral power.

We start with making a list of the proposed coupling functions and their correlation coefficients with the nightside auroral energy deposition in Table 3, where θ_c is the IMF clock angle. Among the list, $VB_T\sin(\theta_c/2)$ is the magnetospheric electric field in the $y-z$ (transverse) plane [*Gonzales and Mozer*, 1974] as well as $VB_T\sin^2(\theta_c/2)$ [*Kan and Lee*, 1979]; $VB^2\sin^4(\theta_c/2)$ is proportional to the energy coupling function, ϵ, proposed by *Perreault and Akasofu* [1978] with the assumption that energy coupling is through the exchange of magnetic energy flux; $P^{1/3}VB_T^2\sin^4(\theta_c/2)$ and $P^{1/6}VB_T\sin^4(\theta_c/2)$ are two alternatives of the energy coupling function with the assumption that the amount of energy which is transferred from the solar wind to the magnetosphere is proportional to the amount of solar wind kinetic energy that is intercepted by an energy "collection" region on the magnetopause [*Vasyliunas et al.*, 1982; *Bargatze et al.*, 1986]. From Table 3 one can see that correlation coefficients at the 60 min lag are always higher than those at the zero lag. This is due mainly to that the IMF B_z correlation coefficient peaks around the 60 min time lag. If we use the correlation coefficient of 0.5 as a landmark given by B_z at the 60 min lag, we can see that the correlation is slightly higher when B_z is combined with the solar wind speed ($r = 0.52$) and the square of solar wind speed ($r = 0.53$). The east-west component of solar wind electric field, VB_z, is much better correlated with the nightside aurora than the transverse component of solar wind electric field, VB_T. This is because the aurora is less correlated with the y component of IMF than the z component of IMF. Therefore a functional dependence on the IMF clock angle, $\sin^n(\theta_c/2)$, where $n = 1$, 2, 3, and 4, is often used. These correlation coefficients are also listed in Table 3, and the results are all improved. The *Perreault and Akasofu*'s [1978] energy coupling function, $\epsilon \approx VB^2\sin^4(\theta_c/2)$, is found to be less correlated with the nightside aurora ($r = 0.55$) than is to the solar wind electric field ($r = 0.63$). When an additional pressure term is added [*Bargatze et al.*, 1986], the correlation coefficient for all transmission functions is not improved. This indicates that the solar wind dynamic pressure does not evidently contribute to the nightside auroral activities in our surveyed data set.

A general energy coupling function was derived by *Vasyliunas et al.* [1982] on a theoretical basis and can be expressed as $\sim \rho V^3 L_{\rm CF}^2 F(M_A^2, \theta_c)$, where ρ is the solar wind density, V is the solar wind speed, $M_A = \sqrt{4\pi\rho V^2/B_T^2}$ is the solar wind Alfven Mach number, $L_{\rm CF} = (M_D/4\pi\rho V^2)^{1/6}$ is the Chapman-Ferraro scale length, and M_D is the Earth's magnetic dipole moment. This form can be simplified as $P^{2/3-\alpha}VB_T^{2\alpha}G(\theta_c)$ if one takes $F(M_A^2, \theta_c) = M_A^{-2\alpha}G(\theta_c)$, where $G(\theta_c)$ is only a function of the IMF clock angle and α is the power law index. If we further assume that $G(\theta_c) = \sin^n(\theta_c/2)$, where $n = 0$, 1, 2, 3,..., then we can determine the two free parameters, α and n, by finding the largest correlation coefficient and the smallest absolute fitting error. The result is shown in Figure 8, where solid contours correspond to the correlation coefficients and dashed contours correspond to the average absolute errors from the linear regression. It is interesting to see that the correlation coefficient is about the same for different powers of $\sin(\theta_c/2)$ except for $n = 1$, which shows a local

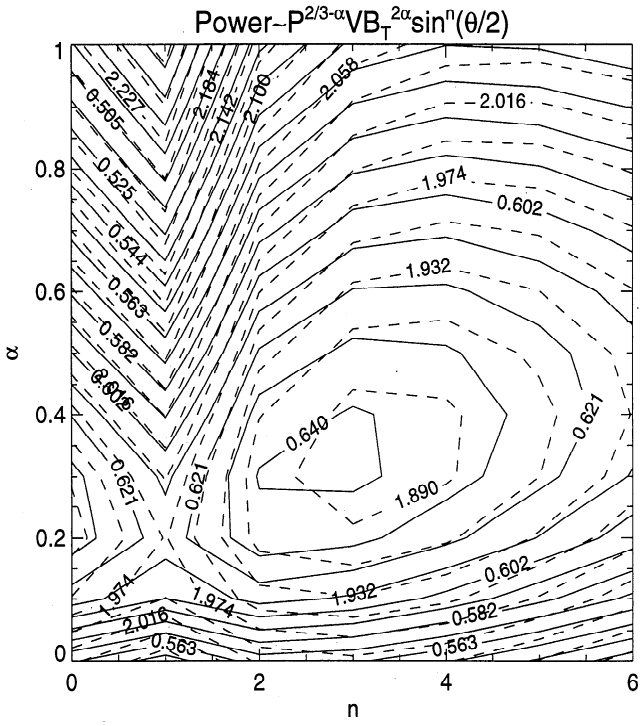

Figure 8. Parametric least squares fit of the nightside auroral power to a solar wind-magnetospheric coupling function, $P^{2/3-\alpha}VB_T^{2\alpha}G(\theta_c)$, where $G(\theta_c) = \sin^n(\theta_c/2)$ is a function of IMF clock angle, θ_c, solid contours correspond to the same correlation coefficients, and dashed contours correspond to the same total absolute errors of the fit.

minimum. Even with $G(\theta_c) = \theta_c$ the correlation coefficient is close to the maximum value for a given α. The change in correlation coefficient with α is more sensitive than that with n. The best regression occurs when the correlation coefficient is the highest and the total absolute fitting error is the lowest. However, in this case, these two extremes are not convergent at the same parameter regime. Therefore we determine the optimum parameter based on the overlapped area, which occurs at about $\alpha = 1/3$ and $n = 3$ for a maximum correlation coefficient of ~0.65.

4. Discussion

Before we proceed to the discussion, we want to point out that the standard deviation is much larger for the sample than for the mean; therefore instantaneous correlation coefficient is much lower. This poor result may be mainly due to an inaccurate estimation of the solar wind plasma and IMF parameters at the ionosphere as discussed in section 2. Although dayside aurora is frequently observed in the afternoon, its transient feature (about a few minutes) may cause a problem for a correlative study with a 5 min temporal resolution like ours (actually, the UVI images used in this survey have 36 s integration time but are separated by about 5 min). Statistical studies with a time resolution of about 1 min or better are necessary in order to acquire a better result. One reason could be internal magnetosphere dynamics. It has been reported that substorms can occur during intervals of steady IMF B_y and B_z components [*Horwitz*, 1985]. Apparently, auroral activities associated with this kind of event do not show any response to the solar wind conditions.

It has been reported that postnoon aurorae appear statistically to be most intense in the 1500 MLT region [*Newell et al.*, 1996b; *Liou et al.*, 1997b] and are collocated with the statistical maximum region 1 upward field-aligned currents [*Iijima and Potemra*, 1976]. Several studies have shown that the occurrence of afternoon arcs is strongly dependent on the existence of a negative B_y component [*Murphree et al.*, 1981; *Vo and Murphree*, 1995; *Karlson et al.*, 1996] but is not significantly dependent on the IMF B_z component [*Vo and Murphree*, 1995]. Our results do show an increase in the total auroral power not only as the IMF B_y becomes more negative but also as the IMF B_y becomes more positive. The z component of the IMF showed a similar effect on the afternoon aurora with the IMF B_y. This may seem to contradict the previous results if one considers that the LBH-long aurorae detected by the UVI imager represent bright, enhanced auroral arcs only. As a matter of fact, diffuse aurorae can be easily detected by the UVI imager and they can sometimes contribute a major part of the emission in the afternoon sector of the auroral oval. However, we believe that the strong IMF dependence of the afternoon auroral power found in this study should mainly reflect the total auroral emission from discrete arcs because diffuse aurorae are persistent and quite stable. Besides, there is not much diffuse aurora at 1500 MLT because electrons drift from nightside toward dawn. Enhanced dayside auroral arcs are usually associated with an enhanced upward field-aligned current and a strong convection reversal in the ionosphere. The duskside convection cell is found to be more crescent shaped for IMF $B_y < 0$ than for IMF $B_y > 0$ [*Ruohoniemi et al.*, 1996]. As a result, stronger upward field-aligned currents and therefore more intense electron precipitation are generally expected. It has been suggested that the IMF B_y may partially "penetrate" into the inner magnetosphere on the dayside [e.g., *Cowley et al.*, 1991; *Newell et al.*, 1995]. *Wing et al.* [1995] reported that the y component of the IMF can partially penetrate the Earth's magnetic field at all local times. At local noon, this penetration was estimated to be ~30% at geosynchronous orbits. This partial penetration of the IMF on the dayside may be responsible for this effect. Since the penetration is expected to be stronger away from the geosynchronous altitude, we expect a none zero curl of the B_y in the z direction. If IMF $B_y > 0$, a southward interhemispheric field-aligned current (into the northern hemisphere) is expected to support this magnetic shear, while if IMF $B_y < 0$, a northward interhemispheric field-aligned current (out of the northern hemisphere) will be produced.

If the southward field-aligned current created by a negative IMF B_y is associated with electron acceleration events or is strong enough (many soft electron precipitation), a brighter dayside aurora will be produced.

Although dayside aurorae are often reported brighter during negative IMF B_y, we found the afternoon auroral output increases with the IMF B_y magnitude as well, and actually, the brightest auroral output occurs when the IMF B_y is large (see Figure 2). The correlation of the afternoon aurora with positive B_y has never been reported. It may suggest a different mechanism which provides a source of precipitating electrons in the afternoon sector. We suggest that the antiparallel merging [*Crooker*, 1979], in particular in the high-latitude region where the Earth's magnetic field lines have footprints in the afternoon region, may be responsible for this IMF B_y effect. The Earth's dipole magnetic fields, when viewed from the north pole in space, are convergent to the center of the Earth. On the duskside, the Earth's magnetic field lines point toward the -y direction and hence favor positive IMF B_y for antiparallel merging. In addition, the IMF B_z and the IMF cone angle dependencies may substantiate the antiparallel merging model responsible for the creation of the afternoon aurora. According to our results, a southward component of the IMF generates more aurorae than a northward IMF in the afternoon. This is consistent with the prediction from reconnection model due to a larger inflow rate near the subsolar point for a more efficient reconnection. Furthermore, a toward orientation of the IMF generates a brighter aurora than an away IMF. This implies a high-latitude reconnection, probably in the plasma mantle where the Earth's magnetic fields point toward the Sun, and therefore favor negative IMF B_x for antiparallel merging.

Dayside auroral activities are generally considered as a consequence of a transient and patchy reconnection proposed by *Berchem and Russell* [1984] and *Kawano et al.* [1992] or a result of an increase in solar wind energy and momentum transfer in the magnetosphere boundary layers due to viscous interaction proposed by *Sonnerup* [1980]. On the basis of this study result, afternoon aurorae show a weak dependence on the solar wind speed and dynamic pressure but a strong dependence on the orientation and the magnitude of IMF and the solar wind electric field, indicating that afternoon aurorae are most likely powered by the solar wind emf due to reconnection in addition to other internal ionospheric/magnetospheric dynamics.

Many early correlative studies have indicated a strong correlation between the southward component of the IMF and geomagnetic disturbances in the high-latitude region [*Arnoldy*, 1971; *Meng et al.*, 1973], and many studies have also suggested a better correlation when the IMF B_z is combined with the solar wind speed [*Rostocker*, 1972; *Murayama and Hakamada*, 1975; *Baker et al.*, 1981]. Although it is impossible to make a quantitative comparison between studies with different proxies of energy input, our statistical results suggest a similar relationship between the auroral power in the midnight sector and the interplanetary quantities. For example, our results indicate that the IMF B_z and the solar wind speed are the two most important parameters which control the nightside aurora, but, in general, the transverse component of the solar wind electric field, $V \times B$, yields a better correlation, so it appears that the solar wind speed dependence is at least partly due to the reconnection. Our results also show a smooth transition from positive IMF B_z to negative IMF B_z. This transition can be approximated by a sine function of the IMF clock angles as suggested by many theoretical works [*Gonzalez and Mozer*, 1974; *Perreault and Akasofu*, 1978; *Kan and Lee*, 1979] and statistical studies [*Bargatze et al.*, 1986; *Scurry and Russell*, 1991]. Many previous works on magnetic disturbances have also found that a peak response of the activity was usually found to occur 40-60 min after the IMF B_z due south, and this delay response was often used to infer a loading magnetosphere. Our results suggesting an average of 60 min delay time for the nightside aurora certainly support the loading-unloading model of the magnetotail. Since our calculation of the time delay for the nightside aurora power is based on the assumption that reconnection that triggers nightside aurora process occurs mainly at the subsolar magnetopause. Generally, this assumption is true for small IMF B_y only. Antiparallel merging may occur at high-latitude magnetopause when the IMF B_y is large and in the nightside mantle area for a northward IMF condition. If this kind of merging can contribute the nightside aurora, then the actual lag time will be shorter. We estimate the error in the response time associated with the high-latitude antiparallel merging is about a few minutes, comparable to the temporal resolution of the UVI images. As the merging site goes to the nightside in the plasma mantle, the error increases to a point that solar wind plasma may not be able to propagate along the opened file lines to the ionosphere because of a large flow shear.

In addition to the above results, we have also found an asymmetry response of the nightside auroral power to the IMF B_y, and it has never been quantitatively identified before. For negative B_y, an average of 15-20% increase in the auroral power over the positive B_y was observed, and it is not dependent on the IMF clock angles. It has been reported that the east-west component of the IMF strongly influences the dayside auroral morphology [*Sandholt et al.*, 1986; *Karlson et al.*, 1996]. The degree of IMF B_y control of the nightside aurora is less clear. This interesting finding may add important information to our knowledge of the way solar wind-magnetosphere-ionosphere interacts and may lead to interesting results. For example, auroral substorms are more intense and more frequent for $B_y > 0$ than for $B_y < 0$ at least as observed in the northern hemisphere, and in a garden hose structure of the IMF, auroral substorms are more intense and more frequent

for a toward orientation than for an away orientation of the IMF.

Similar to the dayside aurora, this B_y effect on the nightside aurora may be related to the nightside ionospheric convection flow which also exhibits a B_y dependence. *Ruohoniemi and Greenwald* [1995, 1996] reported that the dusk convection cell tends to shrink its size into a crescent shape for negative B_y and therefore increases its curvature (vorticity). The plasma flow in the dusk cell moves in a direction such that field-aligned currents are drawn out of the ionosphere. Therefore an increase in vorticity due to negative B_y will result in an increase in the upward field-aligned currents and aurorae. This B_y effect must be associated with reconnection, whereby solar wind electric field is mapped along the open field line to the nightside auroral region. A possible evidence of this is the observation of the penetration of the IMF B_y into the nightside magnetosphere reported by *Lui* [1984] and *Wing et al.* [1995]. Since the degree of the IMF penetration decreases away from the geosynchronous orbits, an interhemispheric upward field-aligned current drawn from the nightside northern ionosphere should be expected [*Stenbaek-Nielsen and Otto*, 1997]. This increase in the upward field-aligned current may consequently enhance the dusk convection cell and auroral arcs in the premidnight sector.

According to our correlative analysis, nightside aurorae are correlated better with the solar wind quantities than dayside aurorae. This may be because nightside auroral activities, such as auroral substorms, have a longer timescale (about 1 hour) than the dayside activities, which generally have a characteristic timescale of 1-10 min and which is comparable to the 5 min temporal resolution of our data set. The best correlation coefficient is found to be 0.65 when the auroral power is lagged by 60 min and fit by $P^{1/3}VB_T^{2/3}\sin^3(\theta_c/2)$, on the basis of a theoretically proposed solar wind-magnetosphere coupling function [*Vasyliunas et al.*, 1982]. However, this response function may not be unique because other forms, such as $P^{1/6}VB_T\sin^4(\theta_c/2)$ and $VB_T\sin^4(\theta_c/2)$ give a similar result ($r = 0.63$), and we feel the latter one should represent a better fit to the nightside auroral energy input because it consists 3 parameters instead of 4.

Other factors may affect the nightside aurora as well. For example, it has been recently reported that nightside aurora are strongly influenced by the ionospheric conductivity [*Newell et al.*, 1996; *Liou et al.*, 1997b]. To test the ionospheric conductivity effect, we simply divide our database by two, before and after June 1, and perform the same correlation analysis. We found that the June-July data set gives a lower-correlation coefficient ($r = 0.57$) compared to the March-May data set ($r = 0.69$). The afternoon aurora also shows a relatively lower-correlation coefficient ($r = 0.28$) for the summer season than for the spring season ($r = 0.45$) when correlated with the solar wind electric field. The small-correlation coefficient in the summer season is consistent with the concept that the increase in ionospheric conductivities due to sunlight takes some control in the production of dayside and nightside aurora.

5. Summary and Conclusion

Total energy deposition rate from precipitating electrons in the northern auroral region inferred by the Polar ultraviolet images at the LBH-long band has been derived to study the response of the dayside/nightside aurorae under various solar wind plasma and IMF conditions. Although subject to large uncertainty, our statistical results indicated that dayside aurorae in the 1300-1800 MLT region have the following characteristics in terms of the solar wind plasma and IMF conditions:

1. The solar wind dynamic pressure, density, and speed do not significantly affect the total intensity of the afternoon aurora.

2. Enhancement of the afternoon aurora appears for a large-transverse component of the IMF and for an away component of the IMF B_x from the Sun.

3. Afternoon aurorae are more active at large IMF cone angles than at small IMF cone angles but with a peak around 100°.

4. The transverse component of the solar wind electric field, $V \times B$, presents a best fit to the total intensity of the afternoon aurora.

Our results suggested that "intense" dayside aurorae are most likely powered by solar wind electric fields which enter the magnetosphere via field line reconnections at various locations where the Earth's magnetic footprints are connected to the postnoon area. It is also suggested that the negative B_y effect may be caused by the partial penetration of the IMF B_y into the dayside closed magnetic field.

The nightside aurora showed a different response to the solar wind and IMF conditions from the afternoon aurora. We can summarize our results as follows:

1. The nightside aurora shows a maximum response to the z component of the IMF when it is lagged by 60 min.

2. Nightside auroral intensity is strongly controlled by the IMF B_z polarity. When $B_z < 0$, the average precipitation power is approximately linearly proportional to the magnitude of the B_z with a slope of 2 GW/nT.

3. A higher nightside auroral intensity was observed for $B_y < 0$ than for $B_y > 0$ in this northern hemisphere database.

4. Nightside auroral intensity is approximately linearly controlled by the solar wind speed.

The 60 min maximum response lag time may indicate that a mechansim of loading-releasing solar wind energy controls the nightside aurora. The strong IMF B_z effect supports the general concept that auroral activities are highly correlated with geomagnetic activities. The negative B_y effect can be explained by the partial penetration of the IMF B_y if the discrete aurora is a consequence of upward field-aligned currents.

The response function for nightside aurora is best represented by $VB_T\sin^4(\theta_c/2)$ with r = 0.63, although a fit to $P^{1/3}VB_T^{2/3}\sin^3(\theta_c/2)$ gives a lightly better correlation coefficient of 0.65.

Acknowledgments. We would like to acknowledge R. P. Lepping as the principal investigator of MFI and K. W. Ogilvie as the principal investigator of SWE. This work was supported by NASA grant NAG 5-3187 to the Johns Hopkins University Applied Physics Laboratory. Research by M. Brittnacher and G. Parks was supported by the NASA grant 5-3170.

The Editor thanks Per Even Sandholt and Harald Frey for their assistance in evaluating this paper.

References

Akasofu, S.-I., and J. R. Kan, Dayside and nightside auroral arc systems, *Geophys. Res. Lett.*, *7*, 753, 1980.

Arnoldy, R. L., Signature in the interplanetary medium for substorms, *J. Geophys. Res.*, *76*, 5189, 1971.

Axford, W. I., and C. O. Hines, A unifying theory of high-latitude geophysical phenomena and geomagnetic storms, *Can. J. Phys.*, *39*, 1433, 1961.

Baker, D. N., Statistical analyses in the study of solar wind-magnetosphere coupling, in *Solar Wind-Magnetosphere Coupling*, edited by Y. Kamide and J. A. Slavin, pp. 17-38, Terra Sci., Tokyo, 1986.

Baker, D. N., E. W. Hones Jr., J. B. Payne, and W. C. Feldman, A high-time resolution study of interplanetary parameter correlations with AE, *Geophys. Res. Lett.*, *8*, 179, 1981.

Bargatze, L. F., R. L. McPherron, and D. N. Baker, Solar wind-magnetosphere energy input functions, in *Solar Wind-Magnetosphere Coupling*, edited by Y. Kamide and J. A. Slavin, pp. 101-109, Terra Sci., Tokyo, 1986.

Berchem, J., and C. T. Russell, Flux transfer events on the magnetopause: Spatial distribution and controlling factors, *J. Geophys. Res.*, *89*, 6689, 1984.

Brautigam, D. H., M. S. Gussenhoven, and D. A. Hardy, A statistical study on the effects of IMF B_z and solar wind speed on auroral ion and electron precipitation, *J. Geophys. Res.*, *96*, 5525, 1991.

Brittnacher, M., R. Elsen, G. Parks, L. Chen, G. Germany, and J. Spann, A dayside auroral energy deposition case study using the Polar Ultraviolet Imager, *Geophys. Res. Lett.*, *24*, 991, 1997.

Burton, R. K., R. L. McPherron, and C. T. Russell, An empirical relationship between interplanetary conditions and *Dst*, *J. Geophys. Res.*, *80*, 4204, 1975.

Cowley, S. W. H., J. P. Morelli, and M. Lockwood, Dependence of connective flows and particle precipitation in the high-latitude dayside ionosphere on the x and y components of the interplanetary magnetic field, *J. Geophys. Res.*, *96*, 5557, 1991.

Crooker, N. U., Dayside merging and cusp geometry, *J. Geophys. Res.*, *84*, 1950, 1979.

Danielsen, C., The dependence of auroral activity upon Kp as determined by the use of an extensive database, *Geophys. Pap. R-60*, Dan. Meteorol. Inst., Copenhagen, 1980.

Doyle, M. A., and W. J. Burke, S3-2 measurements of the polar cap potential, *J. Geophys. Res.*, *88*, 9125, 1983.

Dungey, J. W., Interplanetary magnetic field and the auroral zone, *Phys. Rev. Lett.*, *6*, 47, 1961.

Elphinstone, R. D., K. Jankowska, J. S. Murphree, and L. L. Cogger, The configuration of the auroral distribution for interplanetary magnetic field B_z northward, 1, IMF B_z and B_y dependencies as observed by the Viking satellite, *J. Geophys. Res.*, *95*, 5791, 1990.

Fairfield, D. H., Average and unusual locations of the Earth's magnetopause and bow shock, *J. Geophys. Res.*, *76*, 6700, 1971.

Germany, G. A., M. R. Torr, D. G. Torr, and P. G. Richards, Use of FUV auroral emissions as diagnostic indicators, *J. Geophys. Res.*, *99*, 383, 1994.

Germany, G. A., G. K. Parks, M. Brittnacher, J. Cumnock, D. Lummerzheim, J. F. Spann, L. Chen, P. G. Richards, and F. J. Rich, Remote determination of auroral energy characteristics during substorm activity, *Geophys Res. Lett.*, *24*, 995, 1997.

Gonzalez, W. D., A unified view of solar wind-magnetosphere coupling functions, *Planet. Space Sci.*, *38*, 627, 1990.

Gonzalez, W. D., and F. S. Mozer, A quantitative model for the potential resulting from reconnection with an arbitrary interplanetary magnetic field, *J. Geophys. Res.*, *79*, 4186, 1974.

Holzworth, R. H., and C.-I. Meng, Mathematical representation of the auroral oval, *Geophys. Res. Lett.*, *2*, 377, 1975.

Horwitz, J. L., The substorm as an internal magnetospheric instability: Substorms and their characteristic timescales during intervals of steady interplanetary magnetic field, *J. Geophys. Res.*, *90*, 4164, 1985.

Iijima, T., and T. A. Potemra, The amplitude distribution of field-aligned currents at northern high latitudes observed by Traid, *J. Geophys. Res.*, *81*, 2165, 1976.

Kan, J. R., and L. C. Lee, Energy coupling functions and solar wind magnetosphere dynamo, *Geophys. Res. Lett.*, *6*, 577, 1979.

Karlson, K. A., M. Oieroset, J. Moen, and P. E. Sandholt, A statistical study of flux transfer event signatures in the dayside aurora: The IMF B_y-related prenoon-postnoon asymmetry, *J. Geophys. Res.*, *101*, 59, 1996.

Kawano, H., S. Kokubun, and K. Takahashi, Survey of transient magnetic field events in the dayside magnetosphere, *J. Geophys. Res.*, *97*, 10,677, 1992.

Lassen, K., and C. Danielsen, Quiet time pattern of auroral arcs for different directions of the interplanetary magnetic field in the Y-Z plane, *J. Geophys. Res.*, *83*, 5277, 1978.

Lepping, R. P., et al., The Wind magnetic field investigation, *Space Sci. Rev.*, *71*, 207, 1995.

Liou, K., P. T. Newell, C.-I. Meng, A. T. Y. Lui, M. Brittnacher, and G. Parks, Dayside auroral activity as a possible precursor of substorm onsets: A survey using POLAR ultraviolet imagery, *J. Geophys. Res.*, *102*, 19,835, 1997a.

Liou, K., P. T. Newell, C.-I. Meng, A. T. Y. Lui, M. Brittnacher, and G. Parks, Synoptic auroral distribution: A survey using POLAR ultraviolet imagery, *J. Geophys. Res.*, *102*, 27,197, 1997b.

Lockwood, M., P. E. Sandholt, S. W. H. Cowley, and T. Oguti, Interplanetary magnetic field control of dayside auroral activity and the transfer of momentum across the dayside aurora magnetopause, *Planet. Space Sci.*, *37*, 1347, 1989.

Lui, A. T. Y., Characteristics of the cross-tail current in the Earth's magnetotail, in *Magnetospheric Currents*, *Geophys. Monogr. Ser.*, vol 28, edited by T. A. Potemra, p. 158, AGU, Washington, D.C., 1984.

Lui, A. T. Y., D. Venkatesan, and J. S. Murphree, Auroral bright spots on the dayside oval, *J. Geophys. Res.*, *94*, 5515, 1989.

Maezawa, K., Statistical study of the dependence of geomagnetic activity on solar wind parameters, in *Quantitative Modeling of Magnetospheric Processes*, *Geophys. Monogr. Ser.*, vol. 21, edited by W. P. Olson, p. 436, AGU, Washington, D. C., 1979.

Meng, C.-I., and R. Lundin, Auroral morphology of the midday oval, *J. Geophys. Res.*, *91*, 1572, 1986.

Meng, C.-I., B. Tsurutani, K. Kawasaki, and S.-I, Akasofu, Cross-correlation analysis of the AE index and the interplanetary magnetic field B_z component, *J. Geophys. Res.*, *78*, 617, 1973.

Murayama, T., Coupling function between solar wind parameters and geomagnetic indices, *Rev. Geophys.*, *20*, 623, 1982.

Murayama, T., and K. Hakamada, Effects of solar wind parameters on the development of magnetospheric substorms, *Planet. Space Sci.*, *23*, 75, 1975.

Murphree, J. S., and R. D. Elphinstone, Correlative studies using the Viking imagery, *Adv. Space Res.*, *8*, 9, 1988.

Murphree, J. S., L. L. Cogger, and C. D. Anger, Characteristic of the instantaneous auroral oval in the 1200-1800 MLT sector, *J. Geophys. Res.*, *86*, 7657, 1981.

Newell, P. T., C.-I. Meng, D. G. Sibeck, and R. Lepping, Some low altitude cusp dependencies on the interplanetary magnetic field, *J. Geophys. Res.*, *94*, 8921, 1989.

Newell, P. T., D. G. Sibeck, and C.-I. Meng, Penetration of the interplanetary field B_y and magnetosheath plasma into the magnetosphere: Implications for the predominant magnetopause merging site, *J. Geophys. Res.*, *100*, 235, 1995.

Newell, P. T., C.-I. Meng, and K. M. Lyons, Suppression of discrete aurorae by sunlight, *Nature*, *381*, 766, 1996a.

Newell, P. T., K. M. Lyons, and C.-I. Meng, A large survey of electron acceleration events, *J. Geophys. Res.*, *101*, 2599, 1996b.

Ogilvie, K. W., et al., SWE: A comprehensive plasma instrument for the Wind spacecraft, *Space Sci. Rev.*, *71*, 55, 1995.

Perreault, W. K., and S.-I. Akasofu, A study of geomagnetic storms, *Geophys. J. R. Astron. Soc.*, *54*, 547, 1978.

Reiff, P. H., R. W. Spiro, and T. W. Hill, Dependence of polar cap potential drop on interplanetary parameters, *J. Geophys. Res.*, *86*, 7639, 1981.

Rostoker, G. A., H.-L. Lam, and W. D. Hume, Response time of the magnetosphere to the interplanetary electric field, *Can. J. Phys.*, *50*, 544, 1972.

Ruohoniemi, J. M., and R. A. Greenwald, Observations of IMF and seasonal effects in high-latitude convection, *Geophys. Res. Lett.*, *22*, 1121, 1995.

Ruohoniemi, J. M., and R. A. Greenwald, Statistical patterns of high-latitude convection obtained from Goose Bay HF radar observations, *J. Geophys. Res.*, *101*, 21,743, 1996.

Sandholt, P. T., C. S. Deehr, A. Egeland, B. Lybekk, and R. Viereck, Signatures in the dayside aurora of plasma transfer from the magnetosheath, *J. Geophys. Res.*, *91*, 10,063, 1986.

Scurry, L., and C. T. Russell, Proxy studies of energy transfer to the magnetosphere, *J. Geophys. Res.*, *96*, 9541, 1991.

Sonnerup, B. U. O., Theory of the low-latitude boundary layer, *J. Geophys. Res.*, *85*, 2017, 1980.

Stenbaek-Nielsen, H. C., and A. Otto, Conjugate auroras and the interplanetary magnetic field, *J. Geophys. Res.*, *102*, 2223, 1997.

Strickland, D. J., R. E. Daniel Jr., J. R. Jasperse, and B. Basu, Transport-Theoretic Model for the electron-proton-hydrogen atom aurora, 2, model results, *J. Geophys. Res.*, *98*, 21,533, 1993.

Sugiura, M., and T. A. Potemra, Net field-aligned currents observed by Triad, *J. Geophys. Res.*, *81*, 2155, 1976.

Torr, M. R., et al., A far ultraviolet imager for the international solar-terrestrial physics mission, *Space Sci. Rev.*, *71*, 329, 1995.

Vasyliunas, V. M., J. R. Kan, G. L. Siscoe, and S.-I. Akasofu, Scaling relations governing magnetospheric energy transfer, *Planct. Space Sci.*, *30*, 359, 1982.

Vo, H. B., and J. S. Murphree, A study of dayside auroral bright spots seen by the Viking auroral imager, *J. Geophys. Res.*, *100*, 3649, 1995.

Wing, S., P. T. Newell, D. G. Sibeck, and K. B. Baker, A large statistical study of the entry of interplanetary magnetic field y component into the magnetosphere, *Geophys. Res. Lett.*, *22*, 2083, 1995.

Wygant, J. R., R. B. Torbert, and F. S. Mozer, Comparison of S3-3 polar cap potential drops with the interplanetary magnetic field and models of magnetopause reconnection, *J. Geophys. Res.*, *88*, 5727, 1983.

M. Brittnacher and G. Parks, Geophysics Program, University of Washington, Seattle, WA 98195. (e-mail: britt@geophys.washington.edu)

K. Liou, C.-I. Meng, and P. T. Newell, The Johns Hopkins University Applied Physics Laboratory, 11100 Johns Hopkins Road, Laurel, MD 20723. (e-mail: kan.liou@jhuapl.edu; ching.meng@jhuapl.edu; patrick.newell@jhuapl.edu)

(Received January 6, 1998; revised April 7, 1998; accepted April 21, 1998.)